Size-Dependent Mechanisms in AC Magnetic Hyperthermia Response of Iron-Oxide Nanoparticles

K. D. Bakoglidis, K. Simeonidis, D. Sakellari, G. Stefanou, and M. Angelakeris

Department of Physics, Aristotle University of Thessaloniki, Thessaloniki 54124, Greece

This paper correlates the magnetic properties of iron-oxide nanoparticles in the size range 5–18 nm with the occurring heating loss mechanisms when magnetic nanoparticle colloidal suspensions are subjected to high-frequency ac magnetic fields. The narrow size distribution of the nanoparticles enabled their clear classification into: 1) the superparamagnetic region (as large as 10 nm) where heating is mainly attributed to Néel relaxation; 2) the intermediate superparamagnetic-ferromagnetic transition region (10–13 nm); and 3) the ferromagnetic region (above 13 nm) where hysteresis losses dominate. The results from specific loss power measurements suggest that for size and concentration optimization, superparamagnetic nanoparticles may release significant amounts of heat to the surroundings, while the hysteresis losses mechanism appears to be much more efficient and the heat transfer provided through may be easier tuned for magnetically driven hyperthermia applications.

Index Terms—**Hyperthermia, iron oxides, nanoparticles, relaxation.**

I. Introduction

IRON oxide nanoparticles have become the most common magnetic agents for biomedical applications and especially for specific target heating purposes like ac magnetic field hyperthermia. Their main advantage compared to other phases with stronger magnetic properties (i.e,. zero-valent iron) is their chemical stability in the air or the biological environment, which results to a stabile physiological behavior for long time intervals. In addition, the extensive knowledge about their synthesis in a wide range of sizes and shapes provides the ability for a full control of the obtained magnetic features. Their potential for *in vivo* use is enhanced as a result of their biocompatible nature, injectability, high absorption in the tumor cells, and low protein absorption [1]–[3].

The amount of transferred heat from nanoparticles to the tumor cells is described by the specific loss power (SLP). There is a wide range of SLP values reported for colloidal solutions of iron-oxide nanoparticles depending on the mean size and its distribution, the material's structural and magnetic properties, the role of surfactants and dispersion mediums, the monodispersity and interparticle interactions, the frequency and the intensity of the ac field, or even the conditions of measurement. For instance, the highest reported values correspond to 35 nm magnetosomes (1 kW/g under 10 kA/m and 410 kHz) [4], 16 nm maghemite nanoparticles (1.65 kW/g under 24.8 kA/m and 700 kHz) [5], and strongly interacting 50 nm iron oxide nanoparticles (1.075 kW/g under 86 kA/m and 150 kHz) [6]. On the contrary, in the majority of the cases, lower SLP values in the range 4–100 W/g are usually obtained even for the commercial available nanoparticle dispersions [7]. Accordingly, any kind of comparison should not be performed by just considering the SLP index or the reduced intrinsic loss power, but only after evaluating a series of parameters and ensuring the highest resemblance in experimental conditions.

Below the superparamagnetic limit, iron oxide nanoparticles are easily functionalized and might be guided within biological entities by the application of an external magnetic field. When the field is removed, they return to random orientations resulting in attenuation of net magnetization and thus of collective magnetic behavior that might act as a threat (such as embolism in capillary vessels). Nevertheless, the heating efficiency of superparamagnetic particles in magnetic hyperthermia appears, in general, lower than the one of single-domain ferromagnetic nanoparticles. Therefore, it is expected that the optimum size would lie slightly over the superparamagnetic limit, which is around 15 nm for spherical iron-oxide nanoparticles [5]. It is widely accepted that the mechanisms of heat losses when a high-frequency ac magnetic field is applied to nanoparticles smaller than 20 nm are the moment relaxation (Néel), the particle relaxation (Brown), and hysteresis losses. The Néel mechanism dominates in particles with sizes below 7.5 nm, whereas Brownian mechanism prevails above this diameter, while hysteresis losses beyond superparamagnetic transition [8]. The margins between the regions are not so clearly defined, and researchers suggest a domination region below 20 nm for Néel mechanism and above 20 nm for Brown mechanism [9]. More recent studies support that both Néel and Brown relaxations are overestimated, and actually even weak hysteresis effects may govern the heating procedure [10]. According to this approximation, SLP is expected to present a local maximum within the superparamagnetic size range together with continuously increasing values within the monodomain ferromagnetic region.

This paper aims to investigate the variation of heating losses in the superparamagnetic–ferromagnetic transition region as defined by dc magnetometry experiments in order to provide experimental evidence of the size effect on ac magnetic field heating response and on the corresponding mechanisms dominating in each size range. Spherical iron-oxide nanoparticles in the size range 5–18 nm were produced by thermal decomposition and subjected to ac magnetic hyperthermia measurements. Special care was taken to ensure the highly

Manuscript received August 14, 2011; accepted October 18, 2011. Date of current version March 23, 2012. Corresponding author: M. Angelakeris (e-mail: agelaker@auth.gr).

Color versions of one or more of the figures in this paper are available online at http://ieeexplore.ieee.org.

Digital Object Identifier 10.1109/TMAG.2011.2173474

stability of suspensions and the complete control of interactions during experiments.

II. Experimental

A. Synthesis of Nanoparticles

The preparation of iron-oxide nanoparticles involved the thermal decomposition of $Fe(CO)_5$ in which the synthetic parameters (i.e., the surfactants, the precursors, and the temperature of the procedure) determined the dimensions (5, 8, 10, 13, and 18 nm), the monodispersity, and the size distribution of the obtained nanoparticle colloidal solution [11]. In a typical synthetic procedure for the production of 5 nm nanoparticles, 1.5 mmol $Fe(CO)_5$ was added at 100 °C in 10 mL dioctylether in the presence of 1.5 mmol oleic acid. The mixture was left to reflux for 90 min at 290 °C and then cooled to room temperature. Ethanol was added to yield a black precipitate, which was then separated by centrifugation. The supernatant was discarded, and the particles were redispersed in hexane. By varying the $Fe(CO)_5$-to-oleic-acid molar ratio from 1:1 to 1:4, it was possible to control the mean size in the range 5–13 nm, whereas for the preparation of larger diameters, the precursor's quantity was increased (3 mmol) and a higher reflux period was applied (3 h).

B. Structural and Magnetic Characterization

X-ray diffraction (XRD) and transmission electron microscopy (TEM) were used to identify the iron oxide phases, the particle's morphology, and arrangement. XRD measurements were performed in a Philips PW 1820 diffractometer using Cu K_a radiation. TEM observation were carried out in a 100 kV JEM 100 CX microscope after depositing some drops of the colloidal solutions on carbon-coated copper grids.

Vibrating Sample Magnetometry (VSM: Oxford Instruments 1.2H/CF/HT) was used for the magnetic characterization of the samples, where magnetic loops were recorded at room temperature in order to extract the dependence of magnetization and coercivity on the particle size.

C. AC Magnetic Field Hyperthermia

The thermal response of the samples under an external alternating magnetic field (765 kHz, 11–22 kA/m) was measured by recording the temperature rise of each system during field application. A volume of 2 mL of the particle's dispersion in a polypropylene tube was placed in the center of a water-cooled induction coil with 23 mm diameter consisting of three turns and connected to an ac field generator of 4.5 kW. Hexane was used as the dispersion medium to maintain a stable suspension of nanoparticles during field exposure. The concentration varied between 0.15–1.2 mg/mL. Corresponding values of SLP were calculated, taking into account corrections for heat losses to the environment [12].

III. Results and Discussion

A. Structure and Morphology

Fig. 1 shows the TEM images of 5, 10, and 18 nm nanoparticles as well as the corresponding size distribution diagrams. Accordingly, the average diameters of 5.1 ± 0.2, 9.8 ± 0.3, and 17.9 ± 0.8 nm were measured for the three samples shown. The observations prove that the preparation method is efficient to produce nanoparticles with spherical shape, very narrow size distribution, and high monodispersity.

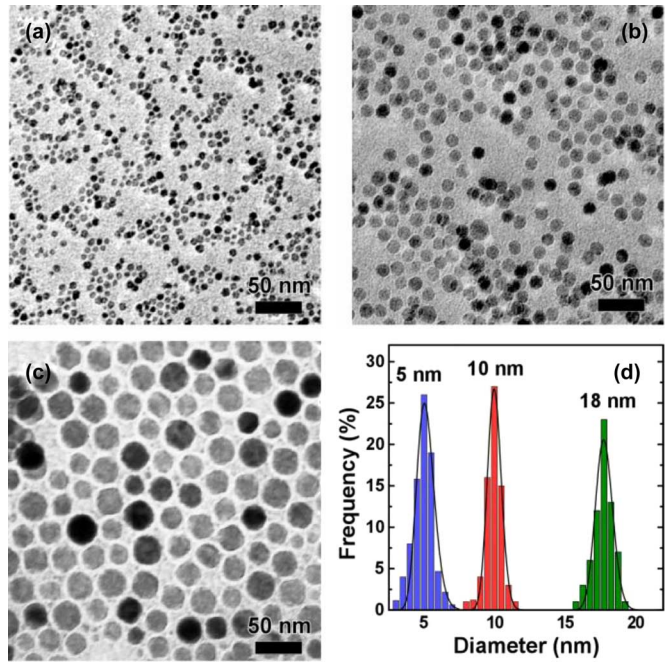

Fig. 1. TEM images of three iron-oxide nanoparticle samples with average size (a) 5, (b) 10, and (c) 18 nm and (d) corresponding size distributions.

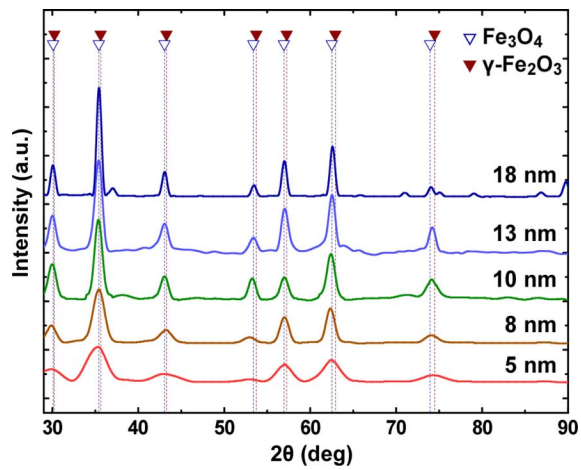

Fig. 2. X-ray diffraction patterns of the samples under study. Broadening of peaks indicates the decrease of nanoparticles' size. Open triangles correspond to the reference reflections for Fe_3O_4, and full triangles to the ones for $\gamma - Fe_2O_3$.

XRD patterns of the prepared samples, presented in Fig. 2, were identified to correspond in Fe_3O_4 and/or $\gamma - Fe_2O_3$. Although a mixture of the two phases should be regarded in all cases, $\gamma - Fe_2O_3$ is expected to dominate in smaller diameters (<8 nm) and Fe_3O_4 at larger ones as the percentage of Fe ions being in the higher oxidation state is proportional to the specific surface area [11]. The mean crystal size of the nanoparticles can be calculated by the broadening of XRD peaks and application of Scherrer's equation. The proximity of these values to the actual diameters of nanoparticles indicates the monocrystalline character of each particle. For instance, mean crystal size was

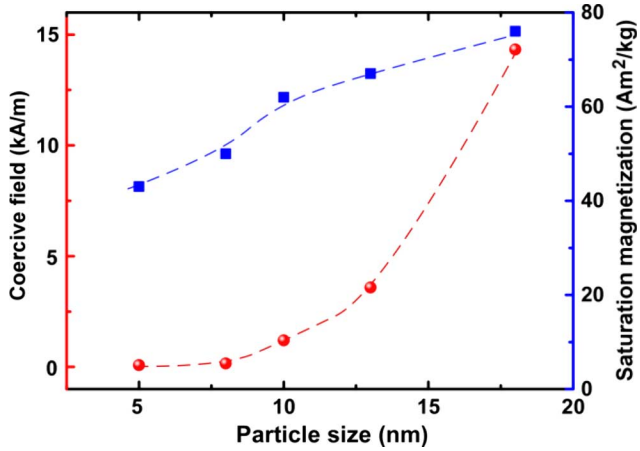

Fig. 3. Size dependence of saturation magnetization and the coercive field for nanoparticles 5–18 nm. Dashed lines serve as guides to the eye.

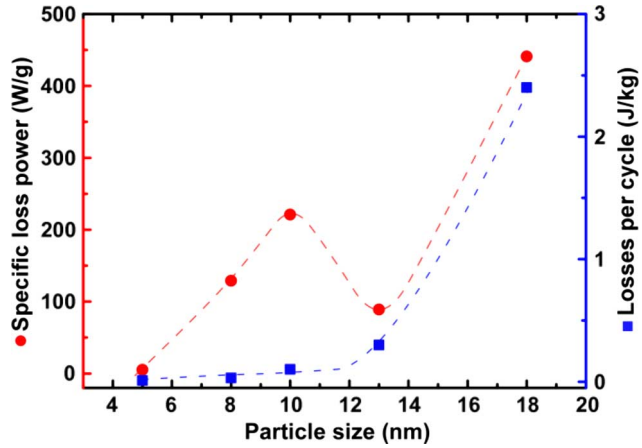

Fig. 4. Dependence of specific loss power and hysteresis losses per cycle versus nanoparticle size, measured for 0.3 mg/mL and ac field of 20 kA/m. Dashed lines serve as guides to the eye.

found to be 5.4 ± 0.4, 9.6 ± 0.7, and 17.4 ± 1.2 nm for the samples appearing in Fig. 1.

B. Magnetic Properties

Hysteresis loops were recorded at room temperature for the various particle sizes, and the parameters describing the magnetic character of the samples were derived. Fig. 3 summarizes the dependence of saturation magnetization and the coercive field on the mean nanoparticle diameter in the range 5–18 nm. At small sizes (<10 nm), coercive field appears to be very close to zero, indicating the superparamagnetic character of nanoparticles. Gradually, coercive field starts to increase when a fraction of the particles is size-distributed beyond the superparamagnetic limit. A clear ferromagnetic behavior is observed for the 18 nm nanoparticles. Saturation magnetization follows a similar trend, getting low values for small particle diameters and trends to bulk magnetization values of iron oxides for larger diameters. The slightly reduced values may be attributed to the asymptotic approximation of saturation in superparamagnetic samples as well as to the increased quantities of surfactants that are proportional to the specific surface area.

From these observations, it is possible to prefigure the heating losses mechanisms when particles' dispersions are subjected to an alternating magnetic field. According to average size range, three regions may be defined: the superparamagnetic region that lies below 10 nm (as almost zero coercivity suggests), the superparamagnetic–ferromagnetic transition region between 10 and 13 nm (gradual increase of coercivity), and the ferromagnetic region for diameters above 13 nm (approaching bulk ferromagnetic values for iron oxides). In particular, since the hysteresis loss is expected to prevail when present, the relaxation models of Néel and Brown should be considered valid only for the net superparamagnetic region.

C. AC Magnetic Hyperthermia Response

The specific loss power was calculated by defining the slope of the temperature rise in the dispersion during ac magnetic field exposure. Fig. 4 shows the measured SLP for nanoparticles dispersions with a concentration of 0.3 mg/mL and an applied ac magnetic field strength of 20 kA/m. It should be mentioned that hexane was intentionally used as a solvent not only to facilitate stability of the nanoparticles due to its high affinity to the surfactant, but, as a low viscous fluid, to restrict friction losses, diminish the Brown relaxation, and eventually restrict the mechanisms of heating in Néel relaxation and hysteresis losses. In any case, the aim of this paper was to provide fundamental experimental information about the physics of heat generation-transfer in monodisperse nanoparticle systems rather than suggesting a dispersion of nanoparticles efficient for hyperthermia application since hexane is not a biocompatible compound.

The variation of SLP in the size range 5–18 nm presents a characteristic local maximum around 10 nm (230 W/g) that corresponds to the critical particle diameter for the Néel relaxation time at the measuring frequency. Below this size, in the net superparamagnetic region, SLP gradually diminishes following the diameter trend, whereas on the other side, it falls to its half-value when the size reaches 13 nm. According to the Néel model, magnetic losses should decrease to zero after the occurrence of the maximum, symmetrically to lower diameters. However, after the turning point at 13 nm, SLP increases rapidly and gets even higher values than the local maximum. This may be comprehended by the appearance of hysteresis losses in the region of superparamagnetism–ferromagnetism transition and their increasing contribution to the heating mechanism. In fact, when the size gets over 10 nm, hysteresis losses seem to dominate very rapidly over the Néel relaxation losses in good agreement with the theoretical maximum heating ability of nanoparticles due to hysteresis, which represents the energy losses per magnetic cycle, calculated by integrating the VSM hysteresis loops at room temperature also shown in Fig. 4 with full squares (right vertical axis). It is evident that hysteresis losses become significant only after the particle size surpasses the superparamagnetic critical diameter, which is beyond 10 nm in these samples.

The described behavior is consistent to recent theoretical models that consider the co-occurrence of Néel and hysteresis mechanisms of heating for the prediction of magnetic losses in various nanoparticle sizes and field strengths [10]. From this point of view, Néel relaxation losses may alternatively be

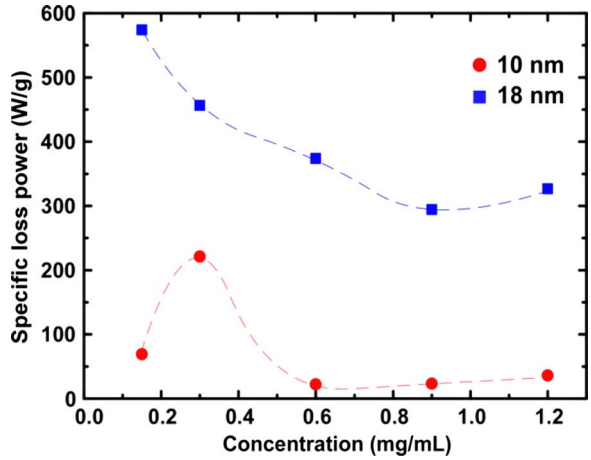

Fig. 5. Specific loss power dependence versus concentration for 10 and 18 nm nanoparticles (ac field 20 kA/m). Dashed lines serve as guides to the eye.

described as common hysteresis losses, but diminishing due to thermal fluctuations. The experimental results prove the success of this model to describe the SLP variation in the superparamagnetic, ferromagnetic, and the transition regions and to take into account the size distribution. The effort to extend the experiments for monodomain nanoparticles larger than 18 nm met many technical problems in the synthetic procedure and the setup of reliable induction heating experiments. For example, the increase of dipolar magnetic interactions expected in ferromagnetic nanoentities and the higher weight of nanoparticles cause a rapid collapse in the stability of nanoparticles dispersion after the application of the ac field.

Another important consideration was derived by the measurement of SLP for different dispersion concentrations in the range 0.15–1.2 mg/mL shown in Fig. 5. For the 18 nm nanoparticles, the heating power appears to present a considerable reduction as concentration increases. This should be expected for ferromagnetic nanoparticles due to the gradual interparticle distance decrease and the appearance of dipolar interactions that cause the enhancement of stability against the magnetic field [13]. The significant effect of particle concentration in the magnetic susceptibility and the hysteresis losses has been recently reported [14]. However, the trend is different for the case of 10 nm nanoparticles where the Néel model is valid. Here, SLP increases at low concentrations, gets a maximum value for around 0.3 mg/mL, and then rapidly diminishes to very small values. This is an indication that concentration may also influence Néel relaxation, which is susceptible to dipolar-dipolar interactions [15]. As a result, the Néel relaxation progressively decreases beyond a concentration value determined by the applied field.

IV. Conclusion

Experimental data concerning the specific heat losses in colloidal dispersions of iron-oxide nanoparticles under high-frequency alternating magnetic field illustrate that single-domain particles in the ferromagnetic region may provide higher heat transfer rates for a wide size and concentration regions. On the other hand, heating losses from superparamagnetic particles may also become significant under certain conditions. However, in the selection procedure of optimum particle size for hyperthermia applications, biocompatibility, dispersion stability, and cell absorption should be also considered.

References

[1] S. Laurent, S. Dutz, U. Hafeli, and M. Mahmoudi, "Magnetic fluid hyperthermia: Focus on superparamagnetic iron oxide nanoparticles," *Adv. Colloid Interfac.*, vol. 166, pp. 8–23, 2011.

[2] Q. A. Pankhurst, N. K. T. Thanh, S. K. Jones, and J. Dobson, "Progress in applications of magnetic nanoparticles in biomedicine," *J. Phys. D, Appl. Phys.*, vol. 42, p. 224001, 2009.

[3] A. Figuerola, R. D. Corato, L. Manna, and T. Pellegrino, "From iron oxide nanoparticles towards advanced iron-based inorganic materials designed for biomedical applications," *Pharm. Res.*, vol. 62, pp. 126–143, 2010.

[4] R. H. R. Hergt, M. Zeisberger, D. Schuler, U. Heyen, I. Hilger, and W. A. Kaiser, "Magnetic properties of bacterial magnetosomes as potential diagnostic and therapeutic tools," *J. Magn. Magn. Mater.*, vol. 293, pp. 80–86, 2005.

[5] J.-P. Fortin, C. Wilhelm, J. Servais, C. Ménager, J.-C. Bacri, and F. Gazeau, "Size-sorted anionic iron oxide nanomagnets as colloidal mediators for magnetic hyperthermia," *J. Amer. Chem. Soc.*, vol. 129, pp. 2628–2635, 2007.

[6] C. L. Dennis, A. J. Jackson, J. A. Borchers, R. Ivkov, A. R. Foreman, J. W. Lau, E. Goernitz, and C. Gruettner, "The influence of collective behavior on the magnetic and heating properties of iron oxide nanoparticles," *J. Appl. Phys.*, vol. 103, p. 07A319, 2008.

[7] M. Kallumadil, M. Tada, T. Nakagawa, M. Abe, P. Southern, and Q. A. Pankhurst, "Suitability of commercial colloids for magnetic hyperthermia," *J. Magn. Magn. Mater.*, vol. 321, pp. 1509–1513, 2009.

[8] R. E. Rosensweig, "Heating magnetic fluid with alternating magnetic field," *J. Magn. Magn. Mater.*, vol. 252, pp. 370–374, 2002.

[9] M. Lévy, C. Wilhelm, J.-M. Siaugue, O. Horner, J.-C. Bacri, and F. Gazeau, "Magnetically induced hyperthermia: Size-dependent heating power of $\gamma - Fe_2O_3$ nanoparticles," *J. Phys. Condens. Matter*, vol. 20, p. 204133, 2008.

[10] R. Hergt, S. Dutz, and M. Zeisberger, "Validity limits of the Néel relaxation model of magnetic nanoparticles for hyperthermia," *Nanotechnology*, vol. 21, p. 015706, 2010.

[11] C. Martínez-Boubeta, K. Simeonidis, M. Angelakeris, N. Pazos-Pérez, M. Giersig, A. Delimitis, L. Nalbandian, V. Alexandrakis, and D. Niarchos, "Critical radius for exchange bias in naturally oxidized Fe nanoparticles," *Phys. Rev. B*, vol. 74, pp. 054430-1–054430-10, 2006.

[12] A. Chalkidou, K. Simeonidis, M. Angelakeris, T. Samaras, C. Martinez-Boubeta, Ll. Balcells, K. Papazisis, C. Dendrinou-Samara, and O. Kalogirou, "In vitro application of Fe/MgO nanoparticles as magnetically mediated hyperthermia agents for cancer treatment," *J. Magn. Magn. Mater.*, vol. 323, pp. 775–780, 2011.

[13] A. Urtizberea, E. Natividad, A. Arizaga, M. Castro, and A. Mediano, "Specific absorption rates and magnetic properties of ferrofluids with interaction effects at low concentrations," *J. Phys. Chem. C*, vol. 114, pp. 4916–4922, 2010.

[14] D. Serantes, D. Baldomir, C. Martinez-Boubeta, K. Simeonidis, M. Angelakeris, E. Natividad, M. Castro, A. Mediano, D.-X. Chen, A. Sanchez, LI. Balcells, and B. Martínez, "Influence of dipolar interactions on hyperthermia properties of ferromagnetic particles," *J. Appl. Phys.*, vol. 108, pp. 073918-1–073918-5, 2010.

[15] Y. Pineiro-Redondo, M. Banobre-Lopez, I. Pardinas-Blanco, G. Goya, M. A. Lopez-Quintela, and J. Rivas, "The influence of colloidal parameters on the specific power absorption of PAA-coated magnetite nanoparticles," *Nanoscale Res. Lett.*, vol. 6, p. 383, 2011.